Physica B 521 (2017) 204–214

Contents lists available at ScienceDirect

Physica B

journal homepage: www.elsevier.com/locate/physb

Structural, elastic and lattice dynamical properties of the alkali metal tellurides: First-principles study

Z. Souadia[a], A. Bouhemadou[a,*], R. Khenata[b], Y. Al-Douri[c,d]

[a] Laboratory for Developing New Materials and their Characterization, Department of Physics, Faculty of Science, University of Setif 1, Setif 19000, Algeria
[b] Laboratoire de Physique Quantique et de Modélisation Mathématique (LPQ3M), Département de Technologie, Université de Mascara, 29000 Mascara, Algeria
[c] Nanotechnology and Catalysis Research Center (NANOCAT), University of Malaya, 50603 Kuala Lumpur, Malaysia
[d] Physics Department, Faculty of Science, University of Sidi-Bel-Abbes, 22000, Algeria

ARTICLE INFO

Keywords:
Alkali metal tellurides
First-principles calculation
Elastic constants
Phonon dispersions
Dielectric properties

ABSTRACT

We report a detailed first-principles density functional calculations to understand the systematic trends for crystal structure, elastic and lattice dynamical properties of the anti-fluorite alkali metal tellurides M_2Te depending from the type of the M cations (M are Li, Na, K and Rb). The calculated equilibrium lattice parameters are in very good agreement with the available experimental data. Single-crystal and polycrystalline elastic moduli and their related properties of the title compounds were calculated via the stress-strain method. The relatively weak values of the calculated elastic moduli demonstrate the weak resistance of these compounds to applied external forces. Phonon dispersion curves throughout the Brillouin zone and corresponding density of states were calculated using the linear response approach. No imaginary phonon modes were found, which indicate the dynamical stability of the examined materials. The atomic displacements at Γ point were determined. Low-frequency dielectric properties and infrared response were investigated.

1. Introduction

The alkali metal chalcogenides M_2Ch [M: Li, Na, K and Rb; *Ch*: O, S, Se and Te], which crystallize in the face-centered cubic antifluorite (anti-CaF_2-type) structure at ambient conditions [1], possess some interesting physical properties, such as high-temperature properties, fast ionic conduction and wide band gap [2–17]. Owing to these aforementioned properties, the M_2Ch materials are potential candidates for several interesting technological applications, such as solid-state batteries [18–20], fuel cells, solid-state gas detectors [21,22] and photo-emissive ultraviolet light materials [23–25]. Among these interesting family members, the alkali metal telluride M_2Te series [M: Li, Na, K and Rb] – the considered compounds – have been the subject of numerous theoretical studies exploring some of their fundamental physical properties. Kikuchiy and co-workers [13] carried out first-principles density-functional calculations on the electronic properties of Li_2Te, Na_2Te and K_2Te using the full-potential linearized augmented-plane-wave (FP-LAPW) method. Seifert-Lorentz and Hafner [26] investigated the structural and electronic properties of K_2Te employing a first-principles pseudopotential plane wave (PP-PW) approach. Eithiraj *et al.* [4] studied the electronic structure of Li_2Te, Na_2Te and K_2Te using the tight-binding linear muffin-tin orbitals (TB-LMTO) method. Kalarasse and Bennecer [9] explored the elastic properties and lattice dynamics of Na_2Te using the PP-PW method. Alay-E-Abbas and co-workers [2,12] studied the structural, electronic and optical properties of the M_2Te [M: Li, Na, K, Rb] series using the FP-LAPW method. Zhang and co-workers [5] investigated the lattice dynamic, thermodynamic and elastic properties of Na_2Te using the PP-PW approach. Bahloul and co-workers [7] studied the structural, electronic and elastic properties of Li_2Te employing the PP-PW approach. Zhang and Shi [10] investigated the lattice dynamics, thermodynamics and elastic properties of Li_2Te through the PP-PW formalism. In spite of these numerous already performed theoretical studies on the alkali metal tellurides M_2Te [M: Li, Na, K, Rb], one can note that a lack of information on some of their physical properties still exists up to now. On one hand, as far as we know, there are no theoretical or experimental investigations of the lattice dynamical, elastic and thermodynamic properties of the K_2Te and Rb_2Te systems. On the other hand, no study was performed to investigate the systematic trends for the structural, elastic, lattice dynamical and thermodynamic properties of the M_2Te family depending from the type of M elements (M are Li, Na, K and Rb). Recently, first-principles investigations of the lattice dynamical and thermodynamic properties of materials have provided some quite satisfactory results [27–33]. In view of these

* Corresponding author.
E-mail addresses: a_bouhemadou@yahoo.fr, abdelmadjid_bouhemadou@univ-setif.dz (A. Bouhemadou).

http://dx.doi.org/10.1016/j.physb.2017.07.004
Received 14 June 2017; Accepted 4 July 2017
Available online 04 July 2017
0921-4526/

circumstances, in the present paper a systematic first-principles study of the structural, elastic and lattice dynamical properties for the M_2Te [M: Li, Na, K and Rb] series was performed using the pseudopotential plane wave method within the generalized gradient approximation.

2. Computational details

All our first-principles calculations were performed within the framework of the density functional theory (DFT) and density functional perturbation theory (DFPT) using the pseudopotential plane-wave (PP-PW) method as implemented in the CASTEP (Cambridge Total Energy Package) code [33]. The electronic exchange and correlation potentials were described using the generalized gradient approximation GGA-PBEsol [34] (it is termed also GGA08), which has been specially developed to improve the description of the exchange-correlation potential in solids. Norm-conserving pseudopotentials [33] were used to describe the interaction potential between the valence electrons and the nucleus and frozen electrons. A plane-wave basis set cut-off of 800 eV and a 15 × 15 × 15 Monkhorst–Pack scheme *k*-points grid [35] for the integration over the Brillouin zone (BZ) were applied to ensure sufficiently accurate total energy calculations. The optimized lattice parameters were calculated by using the Broyden-Fletcher-Goldfarb-Shanno (BFGS) minimization algorithm [36]. The optimized geometry was performed with the following convergence criteria: (i) the total energy difference between two consecutive iterations were smaller than 5.0×10^{-6} eV/atom and (ii) the stress was smaller than 0.02 GPa. The single-crystal elastic constants C_{ij}s were determined from first-principles calculations by applying a set of given homogeneous deformations with a finite value ε and calculating the resulting stress with respect to optimizing the internal atomic freedoms. The C_{ij}s were obtained via linear fittings of the stress-strain curves computed from accurate ab initio calculations [33]; the elastic stiffness tensor is related to the stress tensor and the strain tensor by Hooke's law. To determine the three independent elastic constants C_{ij}s of a cubic system, namely C_{11}, C_{44} and C_{12}, one strain pattern with nonzero ε_{11} and ε_{23} was used. The maximum strain amplitude was set at 0.003. The lattice vibrational properties, namely the phonon dispersion curves, density of phonon states, dielectric tensors and thermodynamic properties were calculated using the linear response method within the density functional perturbation theory (DFPT) [37]. The dielectric tensor and the longitudinal-optical/transverse-optical (LO-TO) splitting are used to calculate the frequency-dependent optical properties in the infrared region (low-frequency region). The phonon frequencies were computed on a 10 × 10 × 10 *q*-points mesh in the BZ.

3. Results and discussion

3.1. Structural properties

At ambient conditions, the M_2Te [M: Li, Na, K, Rb] compounds crystallize in the anti-CaF_2-type structure, space group $Fm\bar{3}m$ (no. 225), with four formula units (Z = 4) per unit-cell [1]. Fig. 1 depicts one unit-cell of the K_2Te compound as a representative of the M_2Te (M: Li, Na, K, Rb) series. The Te atom occupy the Wyckoff position 4*a* (0, 0, 0); the corner and face-centered positions, and the alkali metal atom M are located at the Wyckoff position 8*c* (0.25, 0.25, 0.25), filling the octahedral holes. Therefore, each Te atom is surrounded by eight M atoms and each M atom is attached to four Te atoms as it is shown in Fig. 1 by polyhedrons. Before performing calculations to obtain the elastic constants and lattice vibrational properties of the considered compounds, their equilibrium lattice parameters (a_0) were determined using the above-mentioned settings. Table 1 presents the obtained results along with the available theoretical and experimental data in the scientific literature. Our obtained values for all considered alkali metal tellurides are in excellent accord with the measured ones. Our

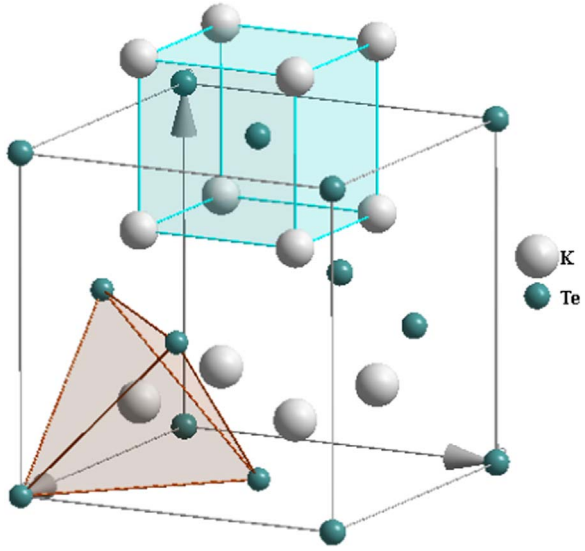

Fig. 1. The centered-faced cubic anti-fluorite Ca_2T-type conventional unit-cell for the K_2Te crystal as representative for the M_2Te [M: Li, Na, K and Rb] series.

calculated values differ from the corresponding measured ones [1,2,26,38] by less than 0.4%, 0.6%, 1.0% and 0.7% for Li_2Te, Li_2Na, Li_2K and Li_2Rb, respectively. Table 1 shows also a good agreement between our results and those from earlier calculations [2,4,5,7,9,10,26]. The lattice parameter a_0 increases with increasing atomic number *Z* of the alkali metal atoms, i.e.,$a_0^{Li_2Te} < a_0^{Na_2Te} < a_0^{K_2Te} < a_0^{Rb_2Te}$. This trend can be attributed to the increase of the atomic radius (*R*) of the alkali metal atom M in the M_2Te series (M: Li, Na, K, Rb) with the increase of their atomic number *Z*, i.e.,$R(Li) < R(Na) < R(K) < R(Rb)$. In order to obtain the bulk modulus *B* and its pressure derivative *B*' values, the calculated primitive-cell volumes (*V*) as a function of pressure for each considered compound are fitted to the Murnaghan equation of state (*EOS*) [39]. The obtained values for *B* and B', listed in Table 1, are in good agreement with the reported data in the scientific literature. The bulk modulus value decreases when going in the following sequence $Li_2Te \rightarrow Na_2Te \rightarrow K_2Te \rightarrow Rb_2Te$, which is in accordance with the Cohen's approximation $B \sim V^{-k}$ [40].

3.2. Elastic constants and related properties

The single-crystal elastic constants C_{ij}s are among the most important parameters that characterize the physical properties of crystals. From a practical point, the elastic constants measure the resistance of a solid to an external applied macroscopic stress and their abilities to recover and regain their original shape after stress ceases. Thus, they provide important information regarding the strength, ductility and hardness of materials. In addition, some macroscopic elastic moduli such as the bulk, Young and shear moduli and Poisson's ratio, which characterize the mechanical properties of solids, can be obtained from the C_{ij}s. From a fundamental viewpoint, the elastic constants are the second derivative of the total energy with respect to strain. Therefore, from the elastic constants, one can derived valuable information on the mechanical stability and the stiffness of the binding between adjacent atomic planes, sound wave velocities, anisotropic character of the bonding, Debye temperature and so on. The computed single-crystal elastic constants C_{11}, C_{12} and C_{44} for the examined systems are quoted in Table 2 as well as available values from other theoretical reports [5,7,9,10] for comparison. The obtained data allow us to make the following conclusions:

(i) No experiments have been conducted out to measure the single-crystal elastic constants C_{ij}s to be compared with our obtained

Table 1
The calculated lattice parameter a_0 (in Å), bulk modulus B (in GPa, derived from the *EOS*) and the pressure derivative of the bulk modulus B' (dimensionless) compared to available theoretical and experimental data in the scientific literature.

	Li_2Te	Na_2Te	K_2Te	Rb_2Te
a_0				
Present work	6.491	7.269	8.068	8.442
Expt.	6.517[a]	7.314[a], 7.329[d]	8.152[a], 8.148[e] 8.168[d]	8.490[b]
Others	6.559[c], 6.478[d] 6.532[d], 6.37[d], 6.483[f], 6.518[g], 6.347[g], 6.518[j],	7.246[c], 7.285[d], 7.383[d], 7.107[d], 7.210[h], 7.209[k]	8.220[c],8.114[d], 8.237[d], 7.919[d], 8.233[e], 8.152[e]	8.460[d], 8.627[d] 8.258[d], 8.233[f]
B (EOS)				
Present work	28.22	20.12	14.83	13.09
Others	26.18[c], 26.84[d], 25.78[d], 33.86[d], 27.18[f],26.03[g], 29.76[g]	21.47[c], 19.72[d], 19.24[d], 22.82[d] 23.61[h], 23.59[k]	13.99[c],12.90[e] 13.78[d], 14.16[d] 17.33[d]	12.08[d], 12.21[d] 14.69[d],
B'				
Present work	3.22	3.91	3.70	3.85
Others	4.68[f], 3.89[g] 3.93[g],	4.41[h], 4.84[k]	4.3[e]	

[a] Ref. [1].
[b] Ref. [38].
[c] Ref. [4].
[d] Ref. [2,12].
[e] Ref. [25].
[f] Ref. [10].
[g] Ref. [7].
[h] Ref. [9].
[k] Ref. [5].

Table 2
The calculated elastic constants (C_{ij}, in GPa), bulk, shear and Young's moduli (B, G, E, respectively, in GPa, derived from the C_{ij}s), Poisson's ratio (σ, dimensionless), anisotropy factor A, universal anisotropy index A^U and anisotropy shear A_{shear} for the Li_2Te, Na_2Te, K_2T and Rb_2Te compounds.

Property	Li_2Te	Na_2Te	K_2Te	Rb_2Te
C_{11}	44.60[a] 46.3[b]	30.06[a], 38.14[c], 38.06[d]	24.58[a]	18.40[a]
C_{12}	16.93[a] 17.62[b]	11.20[a], 16.50[c], 16.17[d]	9.71[a]	7.09[a]
C_{44}	20.57[a] 16.42[b]	14.38[a] 13.15[c], 13.21[d]	8.27[a]	5.81[a]
B (C_{ij})	26.15[a] 27.01[b]	17.49[a] 23.71[c], 23.46[d]	14.67[a]	10.86[a]
G	17.55[a] 15.55[b], 16.92[e], 25.58[e]	12.14[a] 12.25[d]	7.92[a]	5.74[a]
E	43.02[a], 39.19[b] 39.73[e], 61.04[e]	29.58 [a] 38.14[b], 20.46[d]	20.15[a]	14.66[a]
σ	0.2258[a], 0.26[b] 0.174[e], 0.193[e]	0.2180[a], 0.275[d]	0.2711[a]	0.2750[a]
B/G	1.49[a],1.74[b] 1.20[e], 1.30[e]	1.44[a], 1.91[d]	1.85[a]	1.88 [a]
A	1.48 [a] 1.145[b]	1.52[a], 1.21[d]	1.11[a]	1.02[a]
A^U	0.19[a]	0.21[a]	0.013[a]	0.0009[a]
A_{shear}	0.018 [a]	0.021[a]	0.0013[a]	0.00009[a]

[a] Present work.
[b] Ref. [10].
[c] Ref. [9].
[d] Ref. [5].
[e] Ref. [7].

results. However, we can state that there is an acceptable agreement with the available theoretical data for Li_2Te [10] and Na_2Te [5,9] if we take into account that different exchange-correlation potential functionals were used in these different works, which may explain the slight differences between the results.

(ii) For a cubic structure, the mechanical stability of a crystal can be judged via the Born stability criteria [41]:

$$C_{11} + 2C_{12} > 0,\ \ C_{11} - |C_{12}| > 0,\ \ C_{44} > 0 \tag{1}$$

According to the listed data in Table 2, the Born stability criteria (1) are satisfied, implying that these alkali metal tellurides are mechanically stable.

(iii) The C_{ij} values decreases when the alkali metal M atom in the M_2Te series is replaced in the sequence $Li \rightarrow Na \rightarrow K \rightarrow Rb$, indicating the decrease of the stiffness of the M_2Te compounds in the same sequence.

(iv) The relatively weak values of the elastic constants C_{ij}s suggest the weak resistance of these compounds against compressions and shear deformations.

(v) The elastic constant C_{11}, which represents the stiffness against compressional strain, is significantly higher than the C_{44} and C_{12}, which represent the resistance against transverse strain, suggesting that the shear deformation is easier to take place than compression along the principle crystallographic directions.

(vi) The sound wave propagations in a crystal are related to some physical properties such as thermal conductivity. Acoustic wave velocities in a crystal can be obtained from the elastic constants through the resolution of Christoffel equation [42]. In a cubic crystal, the velocities of sound wave propagating in the [100,110] and [111] crystallographic directions are given by the following relationships:

$$V_L^{[100]} = \sqrt{C_{11}/\rho}\,,\quad V_{T1}^{[100]} = V_{T2}^{[100]} = \sqrt{C_{44}/\rho} \tag{2}$$

$$V_L^{[110]} = \sqrt{(C_{11} + C_{12} + 2C_{44})/2\rho}\,,$$
$$V_{T1}^{[110]} = \sqrt{(C_{11} - C_{12})/2\rho}\,,\quad V_{T2}^{[110]} = \sqrt{C_{44}/\rho} \tag{3}$$

$$V_L^{[111]} = \sqrt{(C_{11} + C_{12} + 4C_{44})/3\rho}\,,$$
$$V_{T1}^{[111]} = V_{T2}^{[111]} = \sqrt{(C_{11} - C_{12} + C_{44})/3\rho} \tag{4}$$

The subscripts L and T stand to the longitudinal and transversal polarizations of the propagating sound wave. The computed sound velocities for the considered systems are listed in Table 3.

Table 3
Acoustic wave velocities for different propagating directions (in m/s), isotropic longitudinal, transverse and average sound velocities (V_l, V_t and V_m, respectively, in m/s) and the Debye temperature (Θ_D, in K) for the Li_2Te, Na_2Te, K_2T and Rb_2Te compounds.

	Li_2Te	Na_2Te	K_2Te	Rb_2Te
$V_L^{[100]}$	3603.05	3164.49	3073.38	2363.36
$V_T^{[100]}$	2447.15	2189.23	1782.56	1328.08
$V_L^{[110]}$	3865.70	3415.64	3125.15	2373.31
$V_{T1}^{[110]}$	3603.051	2189.23	1782.56	1328.08
$V_{T2}^{[110]}$	2006.70	1930.74	1690.09	1310.16
$V_L^{[111]}$	3949.37	3571.04	3142.23	2376.62
$V_T^{[111]}$	2315.37	2057.90	1721.46	1316.14
V_l	3797.81	3349.79	3113.98	2371.28
V_t	2261.78	2011.34	1744.97	1320.84
V_m	2502.16	2224.87	1942.13	1470.79
Θ_D	262.78	208.66	164.11	118.76

One can appreciate that the longitudinal wave velocity is larger than the transverse ones and both longitudinal and transverse waves decrease in the same trend as the single-crystal elastic constants because the sound wave velocities are proportional to the square root of the corresponding elastic constants and inversely proportional to the mass density.

(vii) In general, the majority of the synthesized compounds are not single-crystal samples but they are in the form of aggregated mixtures of microcrystallites with random orientations. In these cases, it is not possible to measure the single-crystal elastic constants C_{ij}s but instead of that, isotropic macroscopic mechanical parameters, namely the bulk modulus (B) and shear modulus (G), may be measured. Since polycrystalline elastic moduli are more attractive in technological characterizations of materials, we calculated them from the obtained C_{ij}s. Theoretically, the bulk and shear moduli can be calculated from the C_{ij}s via the Voigt-Reuss-Hill averaging method [43–45]. For a cubic system, the bulk modulus is given by the same formula in both Voigt (B_V) and Reuss (B_R) approximations:

$$B_V = B_R = (\mathbf{C}_{11} + \mathbf{2C}_{12})/3 \quad (5)$$

The Voigt shear modulus (G_V) and Reuss shear modulus (G_R) are defined by the following relationships:

$$G_V = (C_{11} - C_{12} + 3C_{44})/5 \quad (6)$$

$$G_R = 5C_{44}(C_{11} - C_{12})/(4C_{44} + 3(C_{11} - C_{12})) \quad (7)$$

Voigt and Reuss approximations result in the theoretical maximum and minimum values of these two moduli, respectively. According to Hill [45] approximation, the effective B and G moduli are approximated by the arithmetic mean of the two mentioned limits –Voigt and Reuss:

$$B = \frac{1}{2}(B_V + B_R);\ G = \frac{1}{2}(G_V + G_R) \quad (8)$$

The Young's modulus E and Poisson's ratio σ for an isotropic material can be calculated from B and G via the following relationships:

$$E = \frac{9BG}{3B + G};\ \sigma = \frac{3B - 2G}{2(3B + G)} \quad (9)$$

From Table 2, which lists the calculated values of the isotropic moduli: B, G, E and σ, one can make the following conclusions:

a) There is a reasonable agreement between the bulk modulus value calculated from the single-crystal elastic constants C_{ij}s and its corresponding value derived from the *EOS* fit. This may be a proof of the reliability of our predictions for the elastic constants.
b) The relatively weak values of B, which represents the resistance to volume change, G, which represents the resistance to shear deformation, and E, which is defined as the ratio of the tensile stress to the tensile strain, suggest that these compounds are characterized by a weak resistance to applied external stress. The decrease of the values of B, G and E in going from Li_2Te to Rb_2Te is probably due to the increase of the unit-cell volume in the same sequence.
c) Poisson's ratio σ can provide important information regarding the characteristics of the bonding nature. The typical value of σ for ionic crystals is 0.25 [46]. The Poisson's ratio values of the studied materials are close to 0.25, which suggests that the interatomic interactions in these compounds are central and consequently a higher ionic contribution in the interatomic bonding should be assumed.
d) By considering the shear modulus as representing of the resistance to plastic deformation and the bulk modulus as representing of the resistance to fracture, Pugh [47] introduced the B/G ratio as criterion to distinguish between the brittle and ductile character of solids. A low (high) B/G value is associated with brittleness (ductility). According to Pugh's criterion, the critical value of the B/G ratio that separates brittleness and ductility is approximately 1.75 (it corresponds to $\sigma = 0.6$). The B/G ratio values presented in Table 2 suggest that Li_2Te and Na_2Te are brittle while K_2Te and Rb_2Te are ductile. On other hand, Frantsevich *et al.* [48] proposed another criterion, which suggests to classify a compounds as ductile if $\sigma > 1/3$($\sigma = 1/3$ corresponds to $B/G \approx 2.67$) and brittle if $\sigma < 1/3$. According to this criterion, all the herein considered compounds can be classified as brittle materials, which is in discrepancy with the Pugh criterion for the case of Li_2Te and Na_2Te, illustrating the uncertainty of the concept.

(a) Elastic anisotropy of crystals reflects the anisotropy of their chemical bonding in different crystallographic directions. It is necessary and significant to estimate the elastic anisotropy of materials because it is highly correlated with the possibility to induce microcracks in the materials [49,50] and it has a significant influence on the nanoscale precursor textures in alloys [51]. Therefore, some approaches were developed in order to evaluate the elastic anisotropy in crystals. Three different indicators were used in this work to evaluate the elastic anisotropy of the considered compounds.

1) A usually used anisotropy factor; labelled Ziner's anisotropy index A_Z, is given by the following expression [52]:

$$A_Z = 2C_{44}/(C_{11} - C_{12}) \quad (10)$$

For a completely isotropic crystal, A_Z is equal to the unity; any deviation of A_Z from the unity is an indication of the presence of a certain elastic anisotropy. The magnitude of the deviation of A_Z from the unity is a measure of the degree of the elastic anisotropy in the considered crystal. From Table 2 data, one can note that Li_2Te, Na_2Te and K_2Te have a certain degree of elastic anisotropy while Rb_2Te is practically an isotropic crystal.

2) A measurement of the elastic anisotropy in shearing — so-called percentage of elastic anisotropy in shearing A_G — is given by the following expression [53]:

$$A_G = (G_V - G_R)/(G_V + G_R) \quad (11)$$

The subscript R and V stand to the Voigt and Reuss approximations. A_G is null for the isotropic crystals. The percentages of shear anisotropy of the studied materials are listed in Table 2. Li_2Te ($A_G = 1.8\%$) and Na_2Te ($A_G = 2.8\%$) show a weak anisotropy while K_2Te ($A_G = 0.1\%$) and Rb_2Te ($A_G = 0.0\%$) are very close to the isotropic limit.

3) A measure of the elastic anisotropy accounting for both bulk and shear contributions is quantified by a universal index A^U, defined as follows [54]:

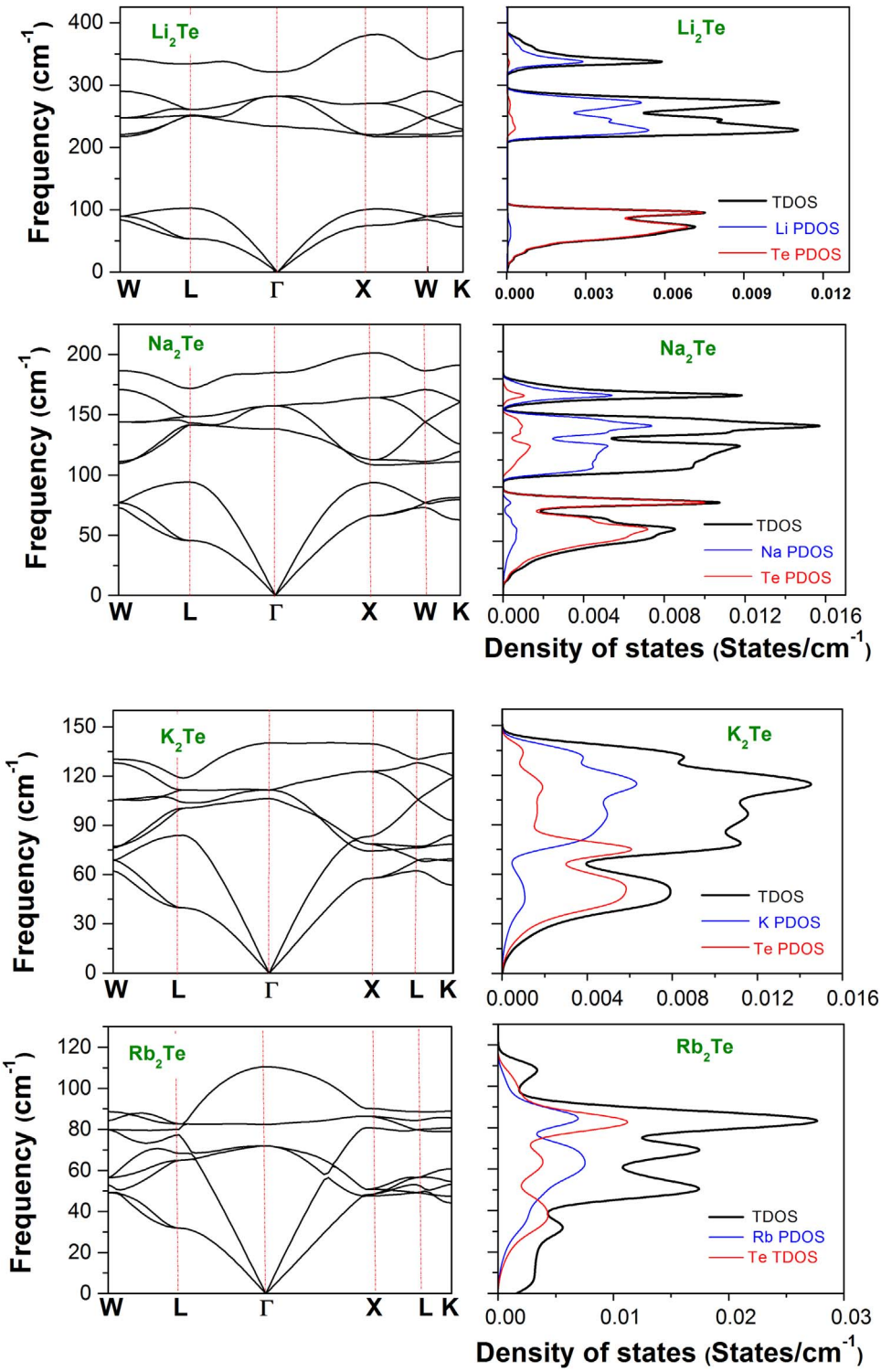

Fig. 2. Calculated phonon dispersion curves and the corresponding total (TDOS) and partial (PDOS) densities of states spectra for the Li_2Te, Na_2Te, K2Te and Rb_2Te compounds.

$$A^U = \frac{5G_V}{G_R} + \frac{B_V}{B_R} - 6, \tag{12}$$

For an isotropic crystal, A^U is equal to zero and any deviation of A^U from zero defines the extent of elastic anisotropy. The numerical estimations of A^U from the calculated values of G_V and G_R for the considered materials are given in Table 2. The obtained results via A^U confirm the already obtained results using other indexes; Li_2Te and Na_2Te show a weak anisotropy while K_2Te and Rb_2Te are very close to the isotropic limit.

(i) Debye temperature θ_D is a fundamental parameter that is closely related to many physical properties of solids, such as specific heat, melting temperature, thermal expansion coefficient, elastic constants and heat conductivity. One of the standard methods to calculate the Debye temperature (θ_D) is from the elastic constants

Table 4
Phonon frequencies at high symmetry points X and L (in cm^{-1}) for the Li_2Te, Na_2Te, K_2Te and Rb_2Te compounds.

	Li_2Te	Na_2Te	K_2Te	Rb_2Te
L_{TA}	53.52[a], 50.93[b]	45.72[a], 46.29[c]	39.73[a]	31.95[a]
L_{LA}	102.80[a], 103.28[b]	94.30[a], 94.83[c]	83.92[a]	64.94[a]
L_{TO1}	250.62[a], 284.57[b]	141.32[a], 153.12[c]	100.50[a]	68.26[a]
L_{LO1}	252.04[a], 287.56[b]	143.14[a], 154.10[c]	103.94[a]	77.30[a]
L_{TO2}	260.78[a], 295.62[b]	148.29[a], 162.60[c]	111.57[a]	80.00[a]
L_{LO2}	334.25[a], 356.65[b]	171.73[a], 179.38[c]	118.77[a]	82.66[a]
X_{TA}	75.34[a], 71.91[b]	66.43[a], 66.93[c]	57.65[a]	47.60[a]
X_{LA}	101.47[a], 105.52[b]	93.78[a], 96.30[c]	74.46[a]	48.16[a]
X_{TO1}	217.35[a], 253.77[b]	108.37[a], 124.95[c]	78.78[a]	50.87[a]
X_{LO1}	220.52[a], 251.72[b]	112.65[a], 120.74[c]	83.25[a]	80.78[a]
X_{TO2}	270.86[a], 308.98[b]	164.23[a], 177.94[c]	122.89[a]	86.35[a]
X_{LO2}	381.47[a], 407.17[b]	201.29[a], 209.89[c]	139.79[a]	90.24[a]

[a] Present work (PP-PW, GGA08).
[b] Ref. [10] (PP-PW, LDA).
[c] Ref. [9] (PP-PW, LDA).

Table 5
The assignment of the vibrational modes, their frequencies (in cm^{-1}) and their activities at the Brillouin zone center for the Li_2Te, Na_2Te, K_2T and Rb_2Te along with available theoretical results.

Symmetry	Li_2Te	Na_2Te	K_2Te	Rb_2Te	Activity
T_g	282.16[a]	157.31[a]	111.60[a]	82.37[a]	Raman
	317.27[b]	169[c], 168[d]			
E_u (TO)	234.05[a]	138.10[a]	106.36[a]	71.94[a]	Infrared
	270.47[b]	152[c,d]			
A_{2u} (LO)	321.24[a]	185.09[a]	140.17[a]	110.42[a]	Infrared
	335.84[b]	190[c,d]			
$\omega_{LO} - \omega_{TO}$	87.19	46.99	34.81	28.05	

[a] Present work (using PP-PW with GGA08).
[b] Ref. [10].
[c] Ref. [9].
[d] Ref. [5] (using PP-PW with LDA).

via the following equation [55]:

$$\theta_D = \frac{h}{k_B}\left[\frac{3n}{4\pi}\left(\frac{\rho}{M}\right)\right]^{\frac{1}{3}} V_m \tag{13}$$

In Eq. (13), V_m is the averaged sound velocity, h is the Plank's constant, k_B is the Boltzmann's constant, ρ is the mass density, n is the number of atoms in the unit-cell and M is the mass of atoms contained in the unit-cell. V_m is given by the following expression:

$$V_m = \left[\frac{1}{3}\left(\frac{2}{V_t^3} + \frac{1}{V_l^3}\right)\right]^{\frac{-1}{3}} \tag{14}$$

Here, V_l and V_t are the longitudinal and transverse elastic wave velocities defined by the following expressions [56]:

$$V_l = \left(\frac{3B + 4G}{3\rho}\right)^{\frac{1}{2}}; \quad V_t = \left(\frac{G}{\rho}\right)^{\frac{1}{2}} \tag{15}$$

The calculated Debye temperature θ_D and the isotropic sound velocities of the investigated compounds are listed in Table 2. The progressive decreasing of the average sound velocities in the M_2Te series in the sequence: $Li_2Te \rightarrow Na_2Te \rightarrow K_2Te \rightarrow Rb_2Te$ explains the lowering of the Debye temperatures in the same sequential order.

3.3. Dynamical properties

3.3.1. Phonon dispersions and density of states

Phonons are the elementary excitations that influence some physical properties especially the thermodynamic behavior. Therefore, a systematic characterization of the phonon density of states and the dispersion relations for the alkali metal tellurides is highly desirable. The calculated phonon dispersion curves along several high symmetry directions in the Brillouin zone (BZ) and the corresponding total and projected atomic phonon densities of states (TDOS and PDOS) spectra for the Li_2Te, Na_2Te, K_2Te and Rb_2Te compounds at the optimized lattice parameters are displayed in Fig. 2. The primitive-cell of the cubic anti-Ca_2F-type structure contains three atoms that give rise to nine phonon modes for a given wave vector q; three are acoustic modes and six are optical ones. Analysis of the calculated phonon dispersion curves and the DOS spectra allows us to make the following conclusions:

(i) No imaginary phonon frequency is observed in the entire BZ, demonstrating that the investigated four alkali metal tellurides are dynamically stable.

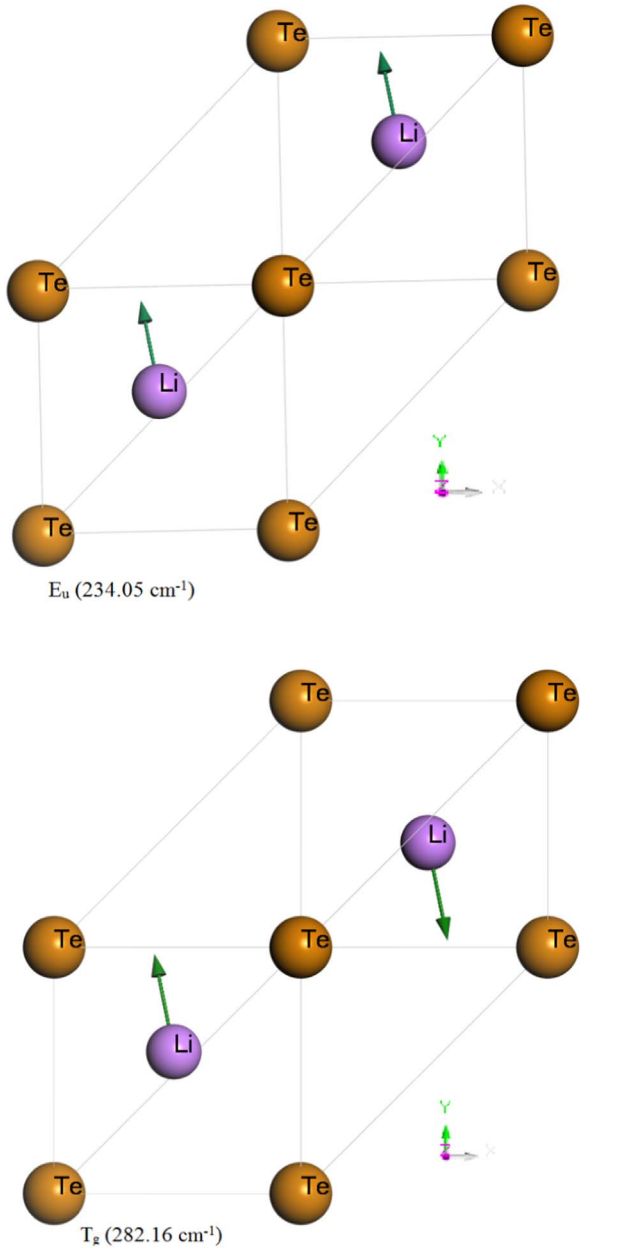

Fig. 3. Schematic representation of E_u (234.05 cm^{-1}) and T_g (282.16 cm^{-1}) optical phonon modes in Li_2Te, with atomic displacements at the Γ point (arrows).

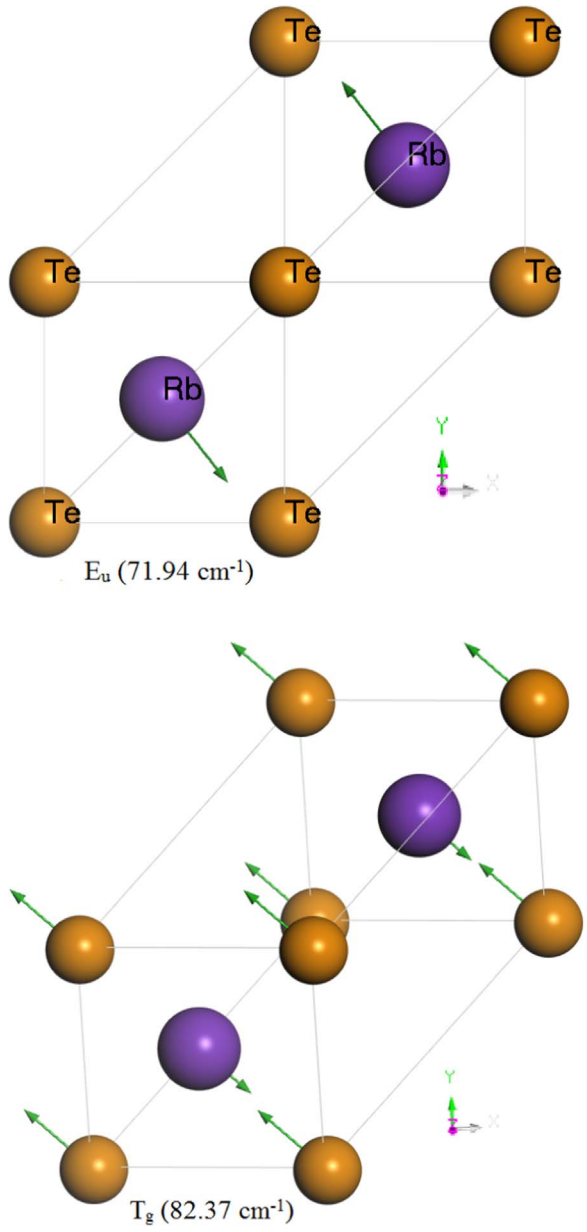

Fig. 4. Schematic representation of E_u (71.94 cm^{-1}) and T_g (82.37 cm^{-1}) optical phonon modes in Li_2Te, with atomic displacements at the Γ point (arrows).

Table 6
Electronic and static dielectric constants (ε_∞ and ε_0, respectively), contribution to the dielectric constant from the IR-active phonon modes (ε_0^{lat}), Born effective charges for the cations (Z^*(M: Li, Na, K, Rb)) and the anions (Z^*(Te)), static refractive index ($n(0)$) and static reflectivity ($R(0)$) for the Li_2Te, Na_2Te, K_2Te and Rb_2Te compounds.

s	ε_∞	ε_0	ε_0^{lat}	n(0)	Z* (M)	Z* (Te)	R(0)
Li_2Te	4.97	9.36	4.39	3.06	1.023	−2.04	0.26
Na_2Te	4.26	7.65	3.39	2.77	1.031	−2.06	0.22
	4.45 [a]				0.954 [a]	−1.908 [a]	
K_2Te	3.53	6.14	2.61	2.48	0.97	−1.95	0.18
Rb_2Te	3.43	6.16	2.73	2.48	1.01	−2.03	0.18

[b] Ref. [9].

(ii) The main features of the obtained phonon dispersion curves are very close to those previously reported for Li_2Te [10] and Ca_2Te [5,9], which were obtained using the PP-PW method with the local density approximation (LDA). We note here that the phonon dispersion curves are available in the scientific literature only for the Li_2Te and Na_2Te compounds. Therefore, this study is the first theoretical prediction of the lattice dynamical properties for the K_2Te and Rb_2Te systems.

(iii) The curves of the longitudinal acoustic (LA) and transverse acoustic (TA) modes have a linear behavior in the neighbouring of the Γ point.

(iv) From Fig. 2, one can observe that the gap between the acoustic and optical branches decreases when going from Li_2Te to Na_2Te to K_2Te to Rb_2Te in the M_2Te series. There is a clear gap between the acoustic and optical branches in the phonon dispersion curves of the Li_2Te and Na_2Te compounds, which merely reflects the large mass difference between the anion Te and the cations Li and Na. The Li_2Te and Na_2Te phonon dispersion spectra exhibit great similarities; the main differences are in the magnitudes of frequencies and the gap separating the optical branches from the acoustic ones. This mentioned gap does not appear at all in the K_2Te and Rb_2Te compounds. Besides, in the Rb_2Te phonon dispersion spectrum, there is an overlapping between the acoustic and optical branches.

(v) The longitudinal optical branch (LO) exhibit an upward dispersion in Li_2Te and Na_2Te, a flat dispersion in K_2Te and a downward dispersion in Rb_2Te along the Γ-X direction while it shows an upward dispersion along the L-Γ direction in the four considered compounds and this dispersion increases from Li_2Te to Rb_2Te.

(vi) The calculated phonon frequencies for the considered compounds at the high symmetry points X, L, W and Γ are summarized in Tables 3, 4. By comparing the phonon frequencies at these mentioned *k*-points, one can appreciate that the substitutions of the alkali metal in the M_2Te series in the sequence: $Li \rightarrow Na \rightarrow K \rightarrow Rb$ causes a downshift of all the phonon frequencies. The width of the phonon band frequencies is approximately 381 cm^{-1} in Li_2Te, 201 cm^{-1} in Na_2Te, 140 cm^{-1} in K_2Te and 110 cm^{-1} in Rb_2Te. The $1/\sqrt{m_{re}}$, where m_{re} is the reduced mass of all the atoms involved in the vibration, is equal to approximately 0.3897 in Li_2Te, 0.2266 in Na_2Te, 0.1828 in K_2Te and 0.1398 in Rb_2Te. These results indicate that the width of the phonon band frequencies is proportional to $1/\sqrt{m_{re}}$. This trend may be attributed to the fact that the frequency of a harmonic oscillator can be calculated from the expression $\omega = \sqrt{\frac{k}{m}}$, where k is the force constant of the bond.

(vii) The total and projected atomic phonon densities (TDOS and PDOS) are depicted in the right panels of Fig. 2. The obtained DOS spectra are in good agreement with the available ones in the scientific literature for the Li_2Te [10] and Na_2Te [5,9] compounds. It is known that the character of the lattice vibrational spectra of solids is governed by both the masses of the constituent atoms and the chemical bonding strengths. One can easily observe that the phonon spectra of the Li_2Te and Na_2Te compounds are divided in two intervals of allowed frequencies separated by an obvious gap. The lower frequency interval, containing only acoustic modes, is attributed to the vibrations of the Te atom while the higher frequency, interval containing only optical modes, is due to the motions of the M (M: Li, Na) atom. The lighter atoms, i.e., Li and Na, move with higher frequencies and the heavier atom, i.e., Te, move with lower frequencies. In the case of K_2Te, one can observe that the low lying optical phonon modes have interaction with the acoustic phonon modes but it is still that the contribution of the Te (K) atom motion is mostly in the acoustic branches (optical branches) and its contribution to the optical branches (acoustic branches) is rather small. In the case of Rb_2Te, these two frequency intervals practically merge and both Rb and Te atom vibrations contribute

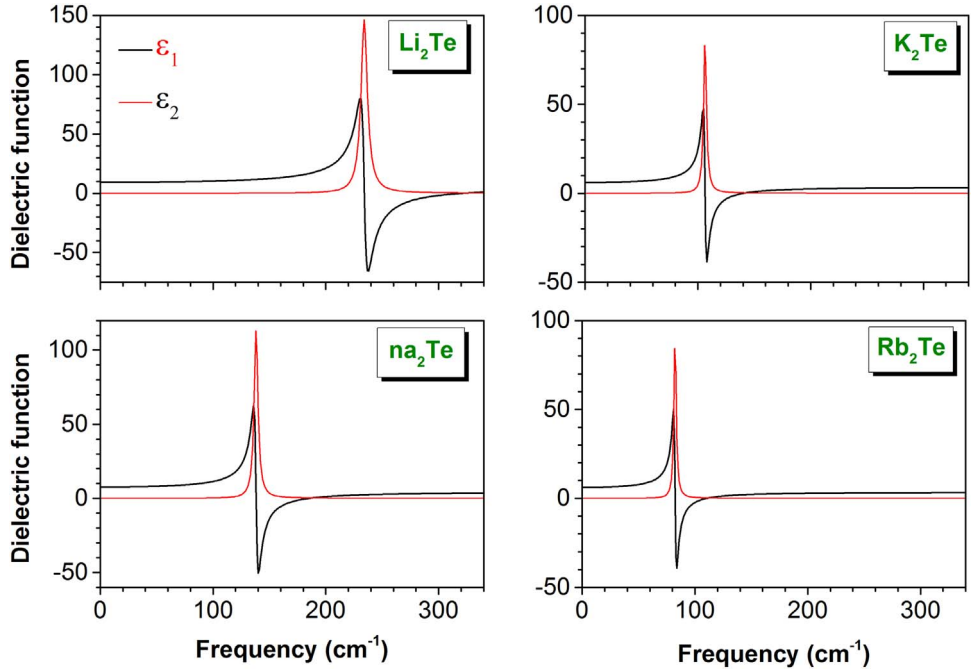

Fig. 5. Calculated real (ε_1) and imaginary (ε_2) parts of the dielectric function dielectric spectra for the Li_2Te, Na_2Te, K_2Te and Rb_2Te compounds. The damping was chosen to be 3% of the frequency.

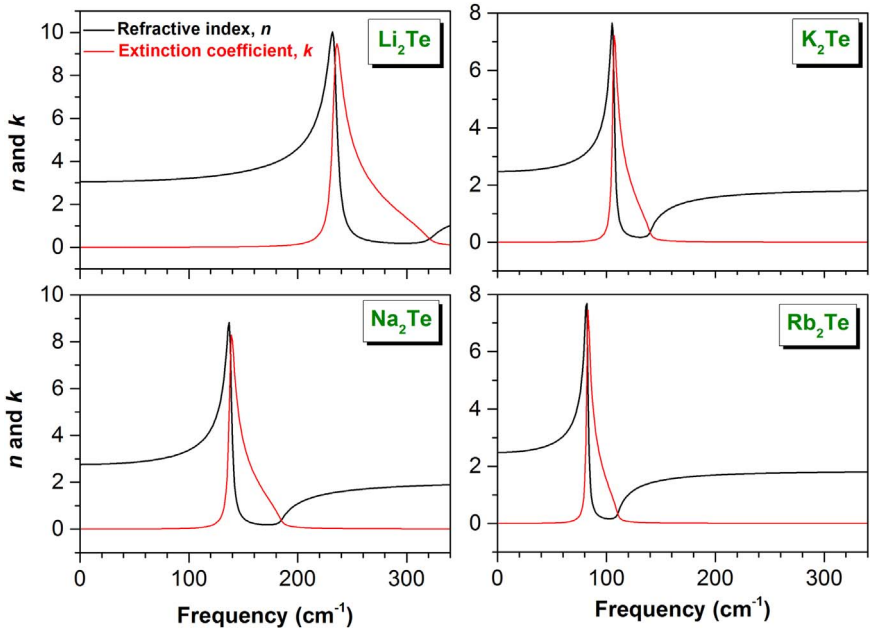

Fig. 6. Calculated infrared refractive index n and extinction coefficient k spectra for the Li_2Te, Na_2Te, K_2Te and Rb_2Te compounds. The damping was chosen to be 3% of the frequency.

with comparably intensities to the acoustic and optical branches. From Fig. 2, one can see that the contributions of the M (M: Li, Na, K, Rb) atom in the lower frequency interval and that of the Te atom in the higher frequency interval increase when going from Li_2Te to Rb_2Te. This indicates that the character of the lattice vibrational spectra of the considered solids is governed by the masses of the constituent atoms.

3.3.2. Zone center phonon and dielectric properties

The lattice vibration modes with $q \approx 0$ play a dominant role in the Raman scattering and infrared absorption. According to the group theory analysis, the irreducible representations of the optical phonon modes at the Brillouin center, Γ point, are:

$$\Gamma_{Optical} = E_u(IR) + T_g(R) + A_{2u}(IR) \quad (16)$$

Here, (IR) stands for infrared-active and (R) for Raman-active, A_{2u} is a single degenerate mode; E_u is a doubly degenerated modes and T_g are triply degenerated modes. The subscripts u and g represent the symmetric mode and the anti-symmetric one in the anti-symmetric center. The calculated phonon frequencies of these vibrational modes are given in Table 5 together with their optical activities and along with the available theoretical results in the scientific literature. Unfortunately, no experimental findings are available in the scientific literature to be compared with our results. The obtained results are in

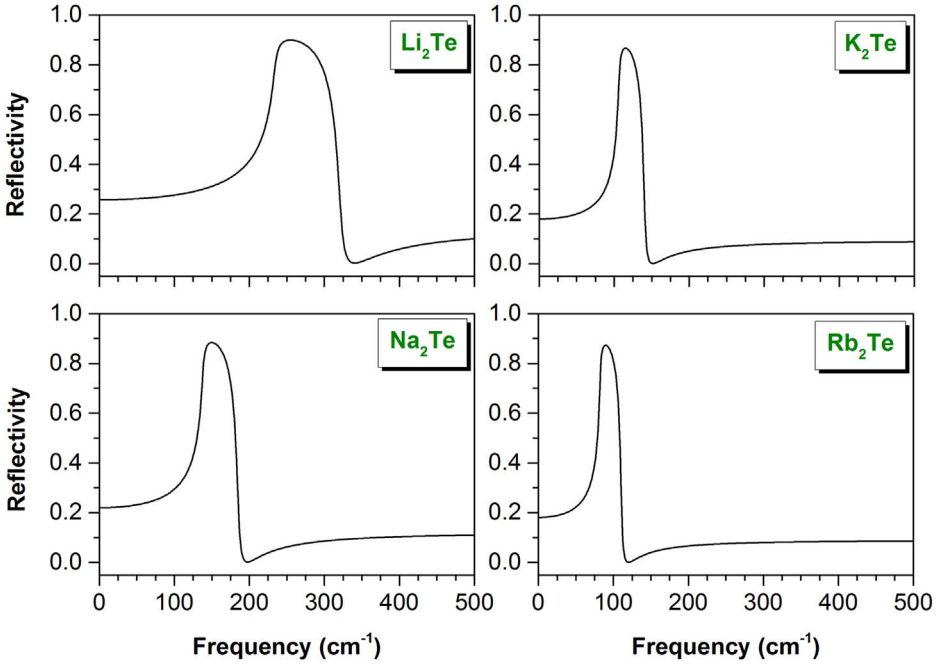

Fig. 7. Calculated infrared reflectance spectra for the Li_2Te, Na_2Te, K_2Te and Rb_2Te compounds. The damping was chosen to be 3% of the frequency.

reasonable agreement with the available theoretical data for the Li_2Te [10] and Na_2Te [5,9] compounds. The triply degenerated phonon mode T_{1g}(without the LO-TO splitting) splits by the macroscopic Coulomb field into E_u(TO) and A_{2u}(LO) phonon modes. The $\omega_{LO} - \omega_{TO}$ splitting is given in Table 5. One can observe that the $\omega_{LO} - \omega_{TO}$ splitting decreases when going from Li_2Te to Rb_2Te in the M_2Te series, indicating that the oscillator strength decreases in the same sequence. Generally, there are two factors that may control the relative positions of the LO and TO frequencies in materials: ionicity and mass ratio between the anion and cation. The LO-TO splitting, which is equal to approximately 87 cm^{-1} in Li_2Te, 47 cm^{-1} in Na_2Te, 34 cm^{-1} in K_2Te and 28 cm^{-1} in Rb_2Te, shows a linear feature when it is plotted as a function of $\sqrt{m_{Te}/m_M}$, where m_{Te} is the mass of the Te atom and m_M is the mass of the M atom (M: Li, Na, K, Rb). The $\sqrt{m_{Te}/m_M}$ is approximately 4.29 in Li_2Te, 2.35 in Na_2Te, 1.80 in K_2Te and 1.22 in Rb_2Te. Thus, we conclude that the LO-TO splitting is mainly influenced by the mass ratio between the cation and anion. It is found that the studied materials have 3 infrared-active optical modes and 3 Raman-active optical modes. From Table 5, one can note that our obtained values are slightly smaller than those reported in the scientific literature. This slight difference may be attributed to the fact that the GGA08 functional used in our work is different from the LDA used in the other calculations; each exchange-correlation potential is known by its own inherent defects. Fig. 3 shows a schematic representation of the optical phonon E_u (234 cm^{-1}) and T_g (282 cm^{-1}) modes in Li_2Te as representative for the M_2Te (M: Li, Na) compounds with the atomic displacements at the Γ point. Fig. 4 shows a schematic representation of the optical phonon E_u (69 cm^{-1}) and T_g (79 cm^{-1}) modes for Rb_2Te as a representative for the M_2Te (M: K, Rb) with the atomic displacements at the Γ point. Only the Li atom vibrations contribute to the optical modes in Li_2Te while both Rb and Te atoms contribute to the T_g optical modes. In the E_u mode, the vibration directions of the neighbouring Li atoms are opposite but in the T_g mode, they move in the same direction.

The low-frequency electronic dielectric ($\varepsilon_{\alpha,\beta}(\infty)$) and the Born effective charges ($Z^*_{\alpha,\beta}$) are defined by the following relationships:

$$\varepsilon_{\alpha,\beta}(\infty) = 1 + 4\pi\frac{\partial P_\alpha}{\partial E_\beta} \tag{17}$$

$$Z^*_{\alpha\beta}(k) = \frac{V}{e}\frac{\partial P_\alpha}{\partial u_\beta(k)} \tag{18}$$

Here, $\boldsymbol{P}$ is the macroscopic electronic polarization by the screened electric field $\boldsymbol{E}$ and $u_\beta(k)$ is the displacement of the k atom. Owing to the cubic symmetry of the considered compounds, the dielectric polarization and Born effective charges are isotropic and consequently the macroscopic electronic dielectric ($\varepsilon_{\alpha,\beta}(\infty)$) and Born effective charges ($Z^*_{\alpha,\beta}$) tensors are diagonal with only one non-zero independent component. The calculated values for the electronic dielectric function ε_∞ and Born effective charges Z* for anions and cations of the examined systems are listed in Table 4 and compared to the available findings in the scientific literature. There is a good agreement between our results and the available data in the scientific literature [9]. Our obtained values for the Born effective charges are very close to the nominal ionic value of −2 for the Te atom and +1 for the M (M: Li, Na, K, Rb) alkali atom. These results demonstrate the strong ionic character of the M-Te bonds and the weakness of the covalent character contributions in these bonds.

3.3.3. Infrared response

Usually, only the contribution of the electronic polarizations to the dielectric function is taken into account when studying the optical properties of materials. However, in the infrared region of the light spectrum – i.e., low frequency electric field –, the ionic materials absorb and reflect light strongly due to the interaction of the electrical field with transverse optical infrared-active phonons [9,57]. Therefore, in the condition of low-frequency electric field, we should take into account both the electronic and ionic polarizations. In this case, the dielectric function is given by the following relationship [57,58]:

$$\varepsilon(\omega) = \varepsilon_1(\omega) + j\varepsilon_2(\omega) = \varepsilon_\infty + \varepsilon_\infty \sum_m \frac{\omega^2_{LO,m} - \omega^2_{TO,m}}{\omega^2_{TO,m} - \omega^2 + j\gamma\omega} \tag{19}$$

Here, $\varepsilon_1(\omega)$ and $\varepsilon_2(\omega)$ are the frequency-dependent real and imaginary parts, respectively, of the dielectric function $\varepsilon(\omega)$, $\omega_{TO,m}$ and $\omega_{LO,m}$ are the transverse and longitudinal optical mode frequencies, respectively, and γ is the damping coefficient. The calculated dielectric spectra of the considered materials in the frequency range 0–350 cm^{-1} are depicted in Fig. 4. In the case of an electrostatic field, the static

dielectric constant ε_0 ($\varepsilon_0 = \varepsilon(0)$) is given by the following expression:

$$\varepsilon_0 = \varepsilon_\infty + \varepsilon_\infty \sum_m \frac{\omega_{LO,m}^2 - \omega_{TO,m}^2}{\omega_{TO,m}^2} \tag{20}$$

The static dielectric constant ε_0 can be also calculated using the Lyddane-Sachs-Teller relationship:

$$\varepsilon_0 = \varepsilon_\infty \prod_m \frac{\omega_{LO,m}^2}{\omega_{TO,m}^2} \tag{21}$$

The calculated static dielectric constants ε_0 for the studied materials and the contributions of the infrared-active phonon modes to ε_0 (ε_0^{lat}) are listed in Table 6. From these obtained results, one can note that the studied M_2Te compounds have an electronic dielectric constant slightly larger than that of the lattice contribution. From the dielectric function dispersion ($\varepsilon(\omega) = \varepsilon_1(\omega) + j\varepsilon_2(\omega)$), one can calculate the dispersion relations for the refractive index $n(\omega)$, extinction coefficient $k(\omega)$ and reflectivity coefficient $R(\omega)$ using the following relationships:

$$\mathrm{n}(\omega) = \sqrt{\frac{1}{2}(\varepsilon_1(\omega) + \sqrt{\varepsilon_1^2(\omega) + \varepsilon_2^2(\omega)})} \tag{22}$$

$$k(\omega) = \sqrt{\frac{1}{2}(-\varepsilon_1(\omega) + \sqrt{\varepsilon_1^2(\omega) + \varepsilon_2^2(\omega)})} \tag{23}$$

$$R(\omega) = \left|\frac{\sqrt{\varepsilon(\omega)} - 1}{\sqrt{\varepsilon(\omega)} + 1}\right|^2 = \frac{(n(\omega) - 1)^2 + k^2(\omega)}{(n(\omega) + 1)^2 + k^2(\omega)} \tag{24}$$

The refractive index $\mathrm{n}(\omega)$ and extinction coefficient $k(\omega)$ spectra of the M_2Te series are depicted in Fig. 5 and the reflectivity $R(\omega)$ spectra are shown in Fig. 6. The static refractive index $\mathrm{n}(0)$ and static reflectivity $\mathrm{R}(0)$ are listed in Table 6. Fig. 6 shows that a strong infrared reflection, higher than 40%, occurs in the range 138–320 cm^{-1} (between ω_{TO} and ω_{LO}) in Li_2Te, 121–183 cm^{-1} in Na_2Te, 97–139 cm^{-1} in K_2Te and 76–110 cm^{-1} in Rb_2Te because the infrared-active modes, resulting in a poor transmission property in this range. The reflectivity attains its maximum (between 85% and 90%) at 255 cm^{-1} in Li_2Te, 150 cm^{-1} in Na_2Te, 115 cm^{-1} in K_2Te and at 89 cm^{-1} in Rb_2Te (Fig. 7).

4. Conclusions

In summary, we investigated the structural, elastic and lattice dynamical properties of a series of alkali metal tellurides with the antifluorite structure, M_2Te (M: Li, Na, K and Te), using the DFT and DFPT with the GGA-PBEsol. The calculated equilibrium lattice parameters fit very well with the measured ones. The calculated single-crystal and polycrystalline elastic constants and their related properties reveal that the examined compounds are mechanically stable and characterized by a weak resistance to external applied strains. The phonon dispersion curves show that the investigated compounds are dynamically stable. The calculated phonon densities reveal that the acoustic modes are due principally to the Te atom vibration and the optical modes are due to the M atom vibration in the Li_2Te, Na_2Te and K_2Te compounds. In Rb_2Te, both atoms Rb and Te contribute comparatively in both acoustic and optical modes. The Raman and infrared frequencies were obtained and assigned using the irreducible representation of the symmetry group at the center of Brillouin zone. The electronic contribution to the dielectric constant is slightly larger than the lattice vibration one. We have investigated the dielectric properties and the infrared response spectra.

References

[1] E. Zintl, A. Harder, B. Dauth, Lattice structure of the oxides, sulfides, selenides and tellurides of lithium, sodium and potassium, Z. Elektrochem. 40 (1934) 588–593.

[2] S.M. Alay-E-Abbas, N. Sabir, Y. Saeed, A. Shaukat, First-principles study of structural and electronic properties of alkali metal chalcogenides: m_2Ch [M: li, Na, K, Rb; Ch: o, S, Se, Te], Int. J. Mod. Phys. B 25 (2011) 3911–3925.

[3] R.D. Eithiraj, G. Jaiganesh, G. Kalpana, M. Rajagopalan, First-principles study of electronic structures and ground-state properties of alkali-metal sulfides – Li_2S, Na_2S, K_2S and Rb_2S, Phys. Status Solidi (b) 244 (2007) 1337–1346.

[4] R.D. Eithiraj, G. Jaiganesh, G. Kalpana, M. Rajagopalan, First-principles study of electronic structures and ground-state properties of alkali-metal selenides and tellurides (M_2A) [M: li, Na, K; A: se, Te, Int. J. Mod. Phys. B 23 (2009) 5027–5037.

[5] X. Zhang, C. Hing, H. Ma, G. Shi, Z. Li, First-principles study on lattice dynamics, thermodynamics and elastic properties of Na_2Te under high pressure, Phys. Scr. 88 (2013) 035602.

[6] R.D. Eithiraj, G. Kalpana, Magnetism induced by nonmagnetic dopant in Li_2O, Na_2O, K_2O and Rb_2O: first-principles calculations, J. Mater. Sci. 47 (2012) 2316–2321.

[7] B. Bahloul, L. Amirouche, A. Dekhira, A. Bentabet, Ab initio study of the structural, electronic and elastic properties of anti-fluorite Li2X (X=S and Te) compounds under pressure effect, Comput. Mater. Sci. 86 (2014) 49–56.

[8] X. Zhang, C. Hing, H. Ma, G. Shi, Z. Li, A first-principles study on lattice dynamics, thermodynamics and elastic properties of lithium selenide under high pressure, Comput. Mater. Sci. 79 (2013) 903–907.

[9] F. Kalarasse, B. Bennecer, Elastic properties and lattice dynamics of alkali chalcogenide compounds Na_2S, Na_2Se and Na_2Te, Comput. Mater. Sci. 50 (2011) 1806–1810.

[10] X.D. Zhang, H.F. Shi, Lattice dynamics, thermodynamics and elastic properties of Li_2Te under high pressure: first principles study, Mater. Sci. Technol. 30 (2014) 732–738.

[11] S.V. Syrotyuk, V.M. Shved, Quasiparticle electronic band of the alkali metal chalcogenides, Condens. Matter Phys. 18 (2015).

[12] S.M. Alay-E-Abbas, A. Shaukat, FP-LAPW calculations of structural, electronic and optical properties of alkali metal tellurides: M2Te [M: li, Na, K and Rb], J. Met. Sci. 46 (2011) 1027–1037.

[13] H. Kikuchiy, H. Iyetomi, A. Hasegawa, Insight into the origin of superionic conductivity from electronic structure theory, J. Phys.: Condens. Matter 10 (1998) 11439–11448.

[14] W. Bührer, H. Bill, Lattice dynamics of Na_2S, J. Phys. C: Solid State Phys. 13 (1980) 5495404.

[15] P.M. Mjwara, J.D. Comins, P.E. Ngoepe, W. Bührer, H. Bill, Brillouin scattering investigation of the high temperature diffuse phase transition in Li_2S, Phys.: Condens. Matter 3 (1991) 4289–4292.

[16] H. Khachai, R. Khenata, A. Bouhemadou, A. Haddou, A.H. Reshak, B. Amrani, D. Rached, B. Soudini, FP-APW+lo calculations of the electronic and optical properties of alkali metal sulfides under pressure, J. Phys: Condens. Matter 21 (2009) 095404.

[17] H. Khachai, R. Khenata, A. Bouhemadou, A.H. Reshak, A. Haddou, M. Rabah, B. Soudini, First principles study of the elastic properties in X_2S (X=Li, Na, K and Rb) compounds under pressure effect, Solid State Commun. 147 (2008) 178.

[18] Hyungjun Noh, Jongchan Song, Jung-Ki Park, Hee-Tak Kim, A new insight on capacity fading of lithium-sulfur batteries: the effect of Li_2S phase structure, J. Power Sources 293 (2015) 329–335.

[19] Md Jamal, G. Venugopal, Md Shareefuddin, M. Narasimha Chary, Sodium ion conducting glasses with mixed glass formers NaI-Na_2O-V_2O_5-B_2O_3: application to solid-state battery, Mater. Lett. 39 (1999) 28–32.

[20] Md Jamal, Md Shareefuddin, M. Narasimha Chary, Ionic transport and battery characterization studies on NaI-Na_20-B_20_3, J. Power Sources 58 (1996) 217–219.

[21] Motohiro Nagao, Akitoshi Hayashi, Masahiro Tatsumisago, Takahiro Ichinose, Tomoatsu Ozaki, Yoshihiko Togawa, Shigeo Mori, Li_2S nanocomposites underlying high-capacity and cycling stability in all-solid-state lithium-sulfur batteries, J. Power Sources 274 (2015) 471–476.

[22] Ki. Bong Lee, Michael G. Beaver, Hugo S. Caram, Shivaji Sircar, Performance of Na_2O promoted alumina as CO_2 chemisorbent in sorption-enhanced reaction process for simultaneous production of fuel-cell grade H2 and compressed CO_2 from synthesis gas, J. Power Sources 176 (2008) 312–319.

[23] Hong-Ki Lee, Joong-Pyo Shim, Mi-Ja Shim, Sang-Wook Kim, Ju-Seong Lee, The characteristics of synthesized potassium hexatitanate and the manufacturing process of the matrix, Mater. Chem. Phys. 45 (1996) 243–247.

[24] D. Bisero, A. Di Bona, P. Paradisi, S. Valeri, K2Te photocathode growth: a photoemission study, J. Appl. Phys. 87 (2000) 543–548.

[25] X. Li, X. Zhao, Z. Chu, Z. Wang, Comparison study of Rb_2Te and Cs_2Te solar blind ultraviolet cathodes, J. Vac. Sci. Technol. 34 (2014) 808–813.

[26] K. Seifert-Lorentz, J. Hafner, Crystalline intermetallic compounds in the K-Te system: the Zintl-Klemm principle revisited, Phys. Rev. B 66 (2002) 094105.

[27] X. Zhang, W. Jiang, Elastic, lattice dynamical, thermal stabilities and thermodynamic properties of BiF_3-type Mg_3RE compounds from first-principles calculations, J. Alloy. Compd. 663 (2016) 565.

[28] X. Zhang, W. Jiang, First-principles investigation on vibrational, anisotropic elastic and thermodynamic properties for L12 structure of Al3Er and Al3Yb under high pressure, Philos. Mag. 96 (2016) 320.

[29] C.–Y. Yang, F.–P. Dai, R. Zhang, L.–H. Li, Q. Zhou, Elastic, phonon and thermodynamic properties of $ZnAl_2O_4$ and $ZnAl_2S_4$ compounds from first–principles calculations, Solid State Sci. 40 (2015) 7–12.

[30] A. Benmakhlouf, A. Bentabet, A. Bouhemadou, S. Maabed, R. Khenata, S. Bin-Omran, Structural, elastic, electronic and optical properties of $KAlQ_2$(Q = Se, Te): a DFT study, Solid State Sci. 48 (2015) 72–81.

[31] U. Koroglu, S. Cabuk, E. Deligoz, First-principles study of structural, elastic, electronic and vibrational properties of $BiCoO_3$, Solid State Sci. 34 (2014) 1–7.

[32] J.-W. Yang, T. Gao, Y.-R. Gong, The disproportionation reaction phase transition, mechanical, and lattice dynamical properties of the lanthanum dihydrides under high pressure: a first principles study, Solid State Sci. 32 (2014) 76–82.

[33] S.J. Clark, M.D. Segall, C.J. Pickard, P.J. Hasnip, M.J. Probert, K. Refson, M.C. Payne, First principles methods using CASTEP, Z. fuer Krist. 220 (2005) 567.
[34] J.P. Perdew, A. Ruzsinszky, G.I. Csonka, O.A. Vydrov, G.E. Scuseria, L.A. Constantin, X. Zhou, K. Burke, Restoring the density-gradient expansion for exchange in solids and surfaces, Phys. Rev. Lett. 10 (2008) 136406.
[35] J.D. Pack, H.J. Monkhorst, Special points for Brillouin-zone integrations, Phys. Rev. B 16 (1977) 1748.
[36] T.H. Fischer, J. Almlof, General methods for geometry and wave function optimization, J. Phys. Chem. 96 (1992) 9768.
[37] K. Refson, P.R. Tulip, S.J. Clark, Variational density-functional perturbation theory for dielectrics and lattice dynamics, Phys. Rev. B 73 (2006) 155114.
[38] K. Stöwe, S. Appel, Polymorphic forms of rubidium telluride Rb_2Te, Angew. Chem. Int. Ed. 41 (2002) 2725–2730.
[39] F.D. Murnaghan, The compressibility of media under extreme pressures, Proc. Natl. Acad. Sci. 30 (1944) 244–247.
[40] M.L. Cohen, Calculation of bulk moduli of diamond and zinc-blende solids, Phys. Rev. B 32 (1985) 7988.
[41] J.F. Nye, Physical Properties of Crystals: Their Representation by Tensors and Matrices, Oxford University Press, Oxford, 1985.
[42] L.D. Landau, E.M. Lifshitz, Theory of Elasticity, Course of Theoretical Physics, Pergamon Press, New York, 1980.
[43] W. Voigt, Lehrbuch der Kristallphysik, B.G. Teubner, Leipzig, Berlin, 1928.
[44] A. Reuss, Berechnung der Fließgrenze, von Mischkristallen auf, Grund der Plastizitätsbedingung für Einkristalle, Z. für Angew. Math. und Mech. 9 (1929) 49–58.
[45] R. Hill, The elastic behaviour of a crystalline aggregate, 1952, Proc. Phys. Soc. A 65 (1952) 349.
[46] J. Haines, J.M. Leger, G. Bocquillon, Synthesis and design of superhard materials, Annu. Rev. Mater. Res. 31 (2001) 1.
[47] S.F. Pugh, Relations between the elastic moduli and the plastic properties of polycrystalline pure metals, Philos. Mag. 45 (1954) 823–843.
[48] I.N. Frantsevich, F.F. Voronov, S.A. Bokuta, I.N. Frantsevich (Ed.)Elastic Constants and Elastic Moduli of Metals and Insulators Handbook, Kiev, Naukova Dumka, 1983, p. 60.
[49] V. Tvergaard, J.W. Hutchinson, Microcracking in ceramics induced by thermal expansion anisotropy, J. Am. Soc. 71 (1988) 157–166.
[50] P. Ravindran, L. Fast, P.A. Korzhavyi, B. Johansson, Density functional theory for calculation of elastic properties of orthorhombic crystals: application to $TiSi_2$, J. Appl. Phys. 84 (1998) 4891.
[51] P. Lloveras, T. Castán, M. Porta, A. Planes, A. Saxena, Influence of elastic anisotropy on structural nanoscale textures, Phys. Rev. Lett. 100 (2008) 165707.
[52] C. Zener, Elasticity and an elasticity of Metals, University of Chicago Press, Chicago, 1948.
[53] H. Chung, W.R. Buessem, in: F.W. Vahldiek, S.A. Mersol (Eds.), Anisotropy in Single Crystal Refractory Compound, 2, New York, 1968.
[54] S.I. Ranganathan, M. Ostoja-Starzewski, Universal Elastic Anisotropy Index, Phys. Rev.
[55] O.L. Anderson, A simplified method for calculating the Debye temperature from elastic constants, J. Phys. Chem. Solids 24 (1963) 909.
[56] E. Schreiber, O.L. Anderson, N. Soga, Elastic Constants and their Measurements, McGraw-Hill, New York, 1973.
[57] X. Zhang, W. Wang, Q. Zeng, H. Li, First-principles study of the dielectric properties and infrared reflectance spectrum of Y_2O_3, Solid State Commun. 150 (2010) 360–363.
[58] V. Zelezny, E. Cockayne, J. Petzelt, M.F. Limonov, D.E. Usvyat, V.V. Lemanov, A.A. Volkov, temperature dependence of infrared-active phonons in $CaTiO_3$: a combined spectroscopic and first-principles, Phys. Rev. B 66 (2002) 224303.